Laboratori Nazionali di Frascati

LNF-74/74(P)

H. C. Dehne, M. A. Preger, S. Tazzari and G. Vignola :

LUMINOSITY MEASUREMENT AT ADONE BY SINGLE AND DOUBLE BREMSSTRAHLUNG

Nuclear Instr. and Meth. 116, 345 (1974)

NUCLEAR INSTRUMENTS AND METHODS 116 (1974) 345-359; © NORTH-HOLLAND PUBLISHING CO.

LUMINOSITY MEASUREMENT AT ADONE BY SINGLE AND DOUBLE BREMSSTRAHLUNG

HANS CHRISTIAN DEHNE

DESY, 2 Hamburg 52, Notkestieg 1, Germany

MIRO ANDREA PREGER, SERGIO TAZZARI and GAETANO VIGNOLA

Laboratori Nazionali del CNEN, Cas. Postale 70, 00044 Frascati, Italy

Received 11 July 1973

The luminosity of the electron–positron colliding beam storage ring Adone has been measured detecting single and double beam–beam bremsstrahlung simultaneously. The two methods are in agreement within experimental errors of the order of ±2.5%. A third luminosity measurement, using small angle Bhabha scattering, was also found to be in agreement with the previous two.

1. Introduction

One of the most important parameters of a colliding beam storage ring is the luminosity L, which is defined as the interaction rate of a process having unit integrated cross section. It is quite obvious that it is desirable for a machine to attain the maximum possible L value. A relative L monitor is therefore needed to monitor machine operation. A relative L monitor is also required by most experiments, but it should be pointed out that absolute L measurements are required by experiments investigating absolute cross sections.

The luminosity of an electron-positron storage ring can be measured by looking at a process of known cross section and high counting rate. Both requirements are met by the following small momentum transfer electromagnetic reactions:

a) $e^+ + e^- \rightarrow e^+ + e^- + \gamma$:
single bremsstrahlung (SB),

b) $e^+ + e^- \rightarrow e^+ + e^- + \gamma + \gamma$:
double bremsstrahlung (DB),

c) $e^+ + e^- \rightarrow e^+ + e^-$:
small angle Bhabha scattering (SAS).

Our apparatus has been designed to measure reactions (a) and (b), while reaction (c) was measured, in the same interaction straight section, by the apparatus described in ref. 1.

Reaction (a) has a very high counting rate: at the characteristic Adone luminosity[2]) of about $10^{33}\,\mathrm{cm^{-2}h^{-1}}$ ($3\times10^{29}\,\mathrm{cm^{-2}s^{-1}}$) the counting rate is of the order of 10 kHz, if γ-rays of energy $E_\gamma \geq 0.1\,E_{max}$ (E_{max} = machine energy) are detected. The angular distribution at our running energies is a narrow peak in the forward direction, so that an experimental aperture of a few milliradians is sufficient to accept almost all outcoming γ-rays: the single bremsstrahlung measurement is therefore almost independent of position and shape of the interaction region. Furthermore, the cross section has a very slow logarithmic dependence on absolute machine energy, so that SB luminosity measurements are almost independent of machine operating conditions. The main source of background is, in the case of Adone, bremsstrahlung on the residual gas (GB); SB and GB cannot be directly separated, but an accurate subtraction can be made on a statistical basis by filling only two of the three buckets available in the machine (see section 4). This procedure of course decreases the luminosity by a factor $\frac{2}{3}$. Actually, luminosity can be measured (under certain conditions, as explained in section 4) provided at least one electron bunch current is different from the other one. The most important source of errors in this kind of measurement is the determination of the detected γ-ray energy threshold. The high counting rate allows SB to be used for "on-line" monitoring of machine operating conditions even when luminosity is very low. These features led us to choose the SB monitor as a machine control facility.

Double bremsstrahlung can be measured under normal machine operating conditions, namely with three bunches in each beam, since two γ-rays are emitted in opposite directions, and can therefore be detected in coincidence. The background arising from both SB and GB accidentals can be subtracted, on a statistical basis, by the usual delayed-coincidence technique. The angu-

lar distribution is peaked in the forward direction, but is not as narrow as that of SB. The measurement is quite sensitive to the aperture of the apparatus, but not to the displacement of the interaction region from the machine axis, or to its longitudinal shape. The uncertainty in threshold determination, which in this case affects both counters, produces an error on luminosity, which is about twice that of the SB measurement. The counting rate is much lower, of the order of ten counts per second. At Adone, DB is mostly useful at low energy under good signal-to-background conditions, since the signal-to-background ratio decreases rapidly with increasing energy (due to increase in gas pressure).

Small angle Bhabha scattering has the great advantage of being very well separable from background events. The only kind of non-separable background is the simultaneous scattering on the residual gas of an electron and a positron: this effect can be subtracted on a statistical basis by means of the delayed-coincidence technique, and it is, in the case of Adone, of the order of 1%. The integrated cross section, however, strongly depends on the longitudinal beam shape (for head-on collisions, which is the normal working condition of Adone), and on the absolute value of the beam energy. A properly designed apparatus can compensate almost exactly for possible displacements of the interaction region from the center of the straight section if the beams cross at an angle (i.e. for small dimensions of the source of the scattering events). In the case of head-on collisions, with longitudinal dimensions of the order of the region seen by the apparatus[3]), compensation becomes much less effective. The measurement is also sensitive to counter alignment, because of the strong angular dependence of the differential cross section. Radiative corrections to small angle scattering are difficult to evaluate, and are a further source of errors. For the actual SAS monitor geometry, the counters being outside the vacuum chamber, the counting rate is of the order of one count per second, under normal operating conditions.

For details on cross sections, signal-to-background ratios, angular distributions, etc., see refs. 4–7.

Our apparatus can measure luminosity at a single crossing point, by measuring SB and DB simultaneously. This paper presents the results of a set of luminosity measurements carried out in March 1972, during a period of approximately one week.

SB and DB were found to be in agreement within the expected experimental errors. Small angle Bhabha scattering, which is a completely independent measurement, was also found to be in agreement within the experimental errors.

2. Experimental setup

Our apparatus consists of three telescopes T1, T2, T3 of one lead–scintillator sandwich and one anticoincidence plastic scintillator (see fig. 1).

Telescopes T1 and T3 are used for SB, while T2 and again T1 are used for DB; T2 is also necessary to correct SB measurements for residual current in the "empty" bunch, as will be explained later. Two windows are provided in the vacuum chamber, one at each side of straight section 11 (interaction section), while at straight section 8, where the bunches do not collide, γ-rays go through the chamber. The original 0.1 mm stainless-steel window had to be replaced (because of synchrotron-radiation problems at beam energies above 1.2 GeV) by 3 mm thick stainless steel ones.

An additional small scintillator counter placed inside bending magnet M10, whose stainless-steel housing projects inside the vacuum chamber, has been occasionally used for tagging purposes.

Sandwich counters are linear up to 1.5 GeV and their

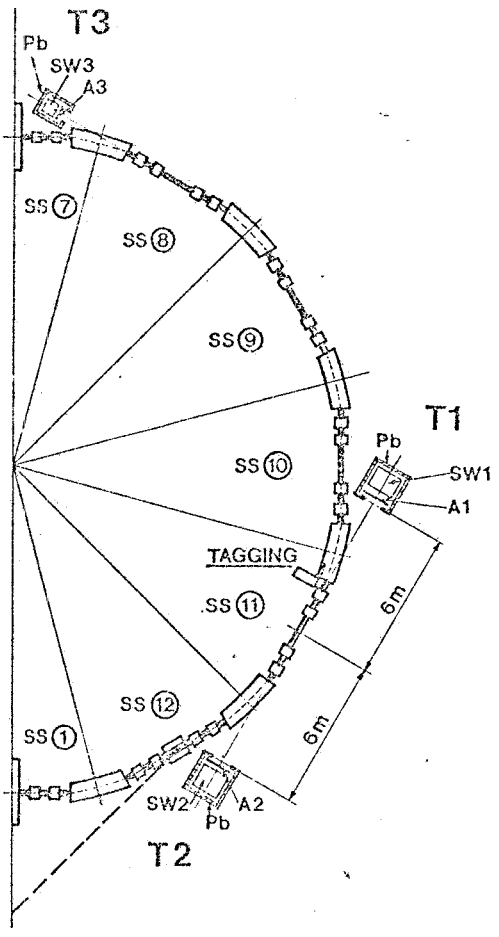

Fig. 1. Experimental layout.

measured resolution (fwhm) is given by the formula:

$$R = \frac{\Delta E}{E} \cong \Gamma\left(\frac{E}{0.4}\right)^{-\frac{1}{2}}, \qquad \Gamma = 0.35, \qquad (1)$$

with E in GeV.

In front of SW1 and SW2 there are two lead collimators defining a half-aperture angle, as seen from the center of the straight section, of 6 mrad. Fig. 2 shows a simplified block diagram of the logics. Since T3 is used only for subtracting background from single bremsstrahlung events, as explained in detail in the following, it does not appear in the diagram.

Counters SW1 and SW2 were aligned with respect to the beam by looking at the outcoming γ-ray beam profiles at the counters; alignment is accurate to ± 0.2 mm both radially and vertically, corresponding to ± 0.03 mrad.

The anticoincidence counters in front of SW1 and SW2 were used

a) to get a clean γ-ray spectrum;

b) to eliminate fringing field effects on the correction for the conversions in the thick window (see section 6); the fringing acts in part as a clearing field, but clearing efficiency changes with beam energy when fixed γ-ray energy thresholds are used.

3. Energy calibration and thresholds

The first problem in connecting SB (or DB) counting rates to luminosity is that of determining the exact value of the threshold energy for γ-ray detection, E_T. We recall that

$$\dot{N}_{SB} = L\int_{E_T}^{E_{max}} \frac{d\sigma(E)}{dE}\, dE,$$

where $d\sigma(E)/dE$ is the differential SB cross section. The value of E_T is of course determined by the discriminator setting (see fig. 2).

E_T can be found by calibrating the GB pulse height spectra:

a) against the theoretical ones, the machine energy being well known,

b) against a tagged spectrum of known energy.

After checking that results obtained through the two methods were in good agreement, we chose to rely, during normal operation, on method (a), which is more practical.

3.1. Calibration method

The thin target energy spectrum of GB γ-rays, in the extreme relativistic case and for complete screening, can be found in ref. 5. Since the spectrum does not change with energy if the reduced variable $\varepsilon = E_\gamma/E_{max}$ is used, we have plotted in fig. 3 the product of ε times the spectral function $n(\varepsilon)$ versus ε. Given the energy resolution of our counters [see eq. (1)], the curves of fig. 3 are obtained by folding R into the theoretical spectrum, for different values of Γ. It can be seen that, since the high-energy part of the GB spectrum is, in the approximations of ref. 5, a step function, all curves with $\Gamma \neq 0$ cross the $\varepsilon = 1$ step at almost exactly the same point, irrespective of the value of Γ (at least for $\Gamma \leqslant 0.6$). Moreover, all spectra have a nearly flat region at around $\varepsilon = 0.65$, so that the following approximate method for finding channel C_M, corresponding to $\varepsilon = 1$ in our pulse height spectrum, can be envisaged: assume y_P to be the ordinate of the flat region (plateau) of the spectrum; C_M is then the abscissa of the point on the spectrum, which has the ordinate

$$y_M = \frac{y_P}{1.82\,(1 \pm 0.013)}.$$

The introduction of a more sophisticated shape for the high-energy side of the spectrum[8]) leads to corrections that are small with respect to the overall accuracy of our reconstruction of spectra, and were accordingly neglected.

We also need to know what channel (C_0) in our pulse height spectrum corresponds to zero energy. By knowing C_0 and C_M, and assuming the pulse height analysis chain is linear, we have an energy calibration of the apparatus, and can therefore proceed to find E_T.

Let us briefly describe how the actual system works: counter pulses enter a linear gate, are superimposed on

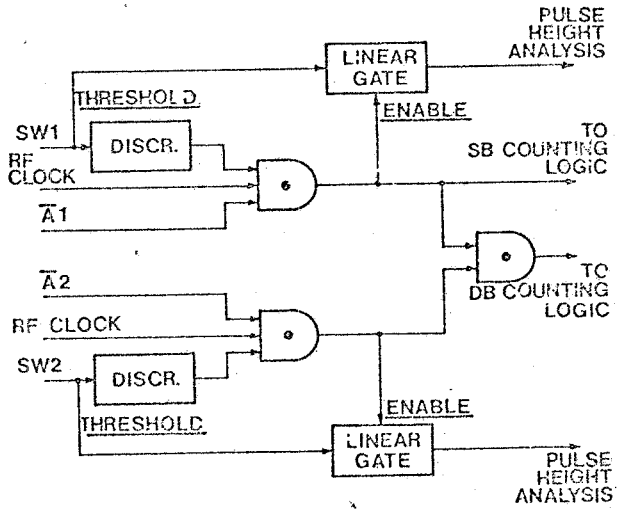

Fig. 2. Simplified diagram of event defining logic.

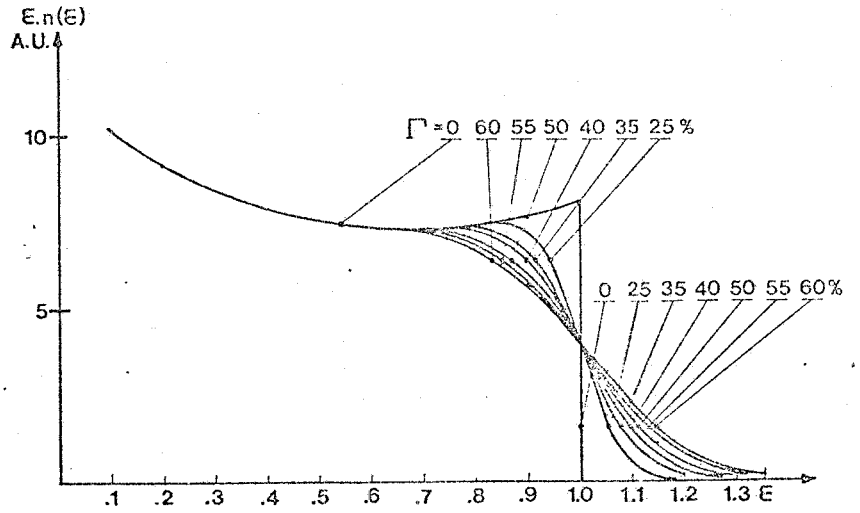

Fig. 3. Differential gas-bremsstrahlung spectrum at a maximum energy of 1 GeV, with resolutions $\Gamma = 0$, 25, 35, 40, 50, 55, 60% at 400 MeV.

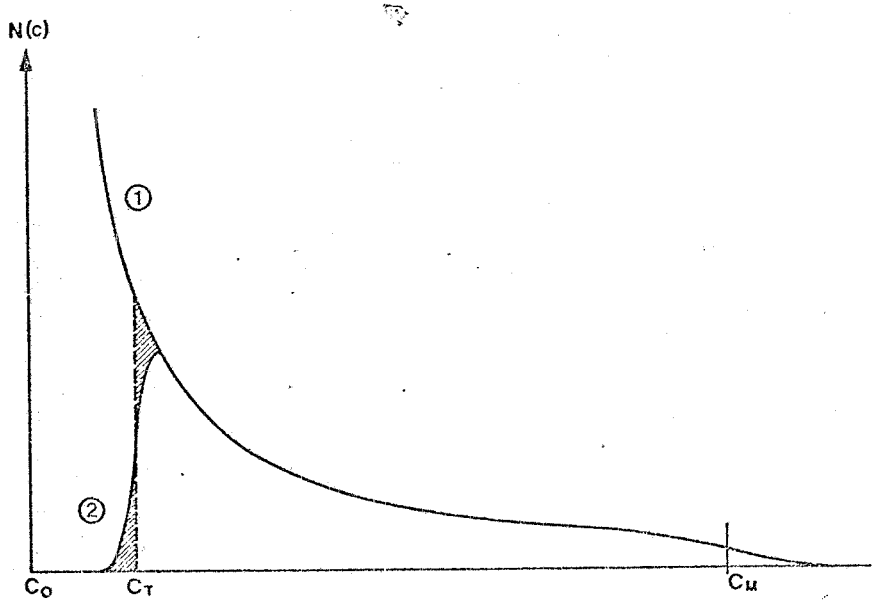

Fig. 4. Method for finding the threshold. Curve 1 is the theoretical spectrum, curve 2 is the experimental one.

a constant amplitude pedestal, and are then fed to a 200-channel pulse height analyzer. An external clock continuously generates "pedestal-only" pulses, which are also fed, during the measurement, to the analyzer. The zero-energy channel C_0 can thus be identified on each spectrum. Once the spectrum is completed, it is directly transferred to a computer, which identifies C_0 and C_M, calculates the calibration factor

$$f = \frac{E_{max}}{C_M - C_0},$$

(the channel width in energy units) and compares the experimental to the theoretical spectrum, by normalizing one to the other at the plateau. Fig. 4 explains how the threshold energy is defined: curve 2 is the experimental spectrum, and curve 1 the theoretical one: the two curves are normalized to each other at one point on the plateau; C_T is defined by the following condition:

$$\int_{C_T}^{\infty} N(C)_{th}\,dC = \int_{0}^{\infty} N(C)_{exp}\,dC,$$

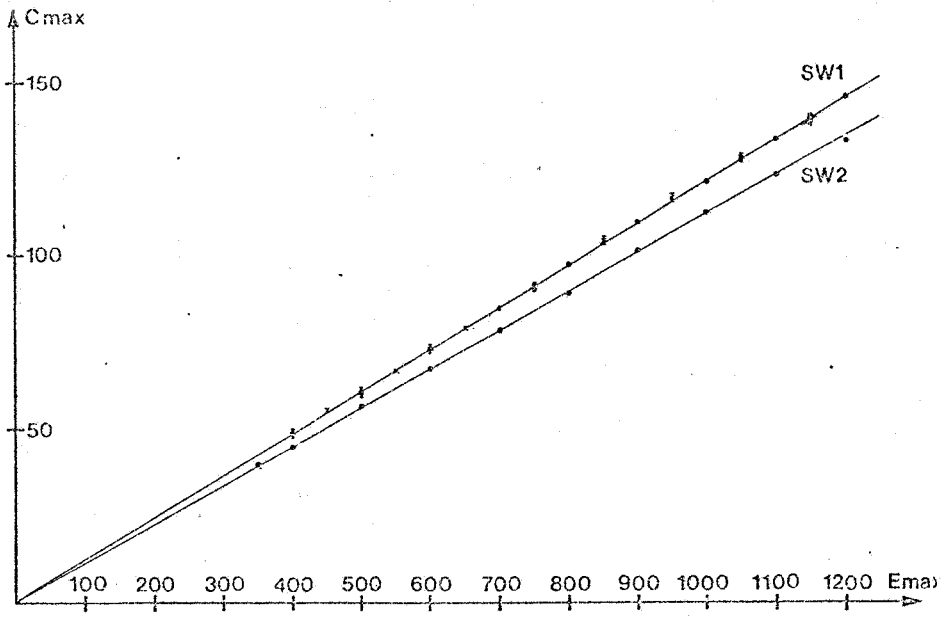

Fig. 5. Linearity of pulse-height analysis chains.

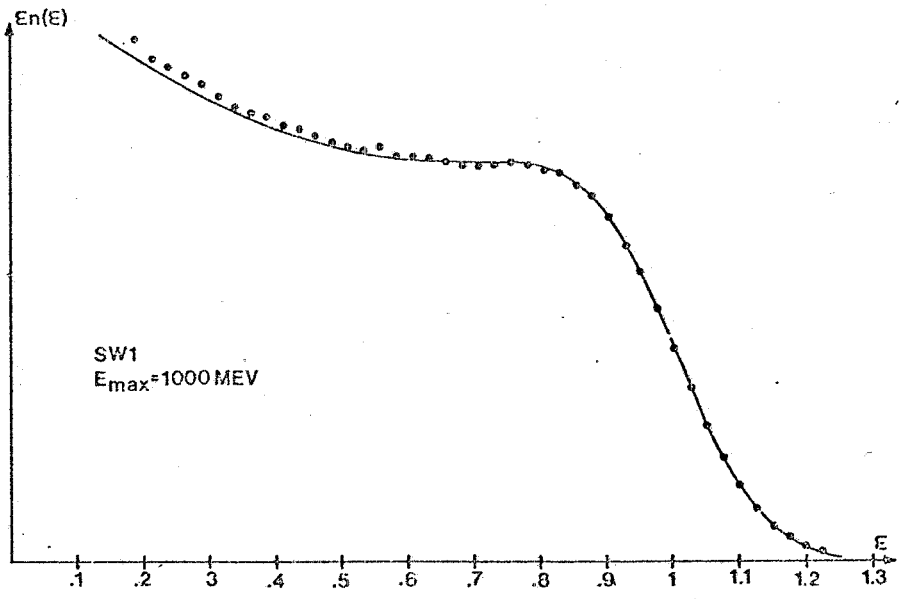

Fig. 6. Experimental gas-bremsstrahlung spectrum compared with theoretical spectrum for SW1. Beam energy 1 GeV.

and E_T is then given by

$$E_T = f(C_T - C_0).$$

3.2. Linearity of detectors and analyzing system

The sandwich counters were tested in a monoenergetic beam of 100–700 MeV electrons. They were found to be linear to within the experimental errors in this range, and energy resolution was found to vary as the square root of energy, as expected, being 35% fwhm at 400 MeV. More accurate tests of the whole chain, in the 350–1200 MeV range, were performed at the storage ring, using the GB beam (see fig. 5).

Linearity of the electronics has been tested using a pulser. Differential and integral linearities have been

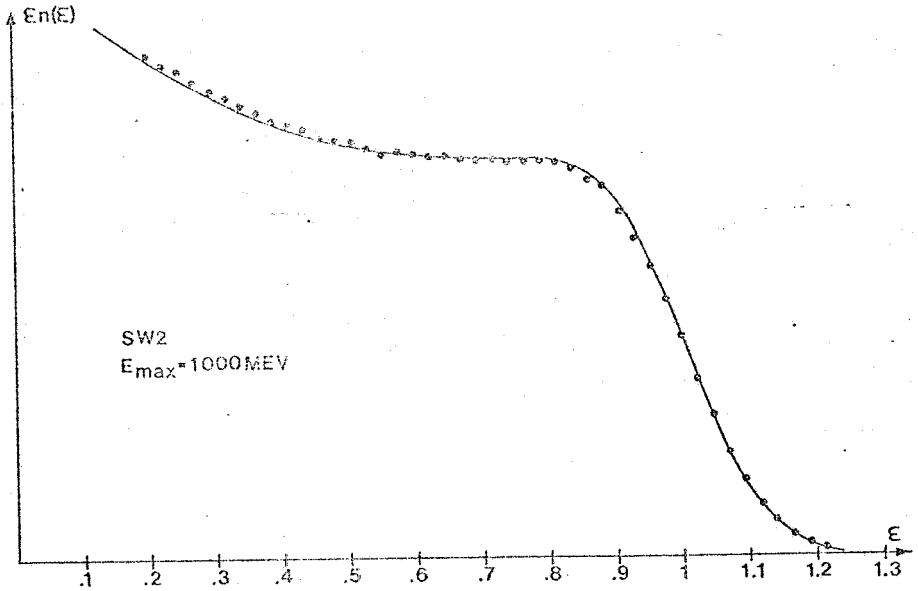

Fig. 7. Experimental gas-bremsstrahlung spectrum compared with theoretical spectrum for SW2. Beam energy 1 GeV.

found to be within ± 0.3 channels, which is compatible with the pulse height analyzer specifications. Fig. 5 shows the linearity of SW1 and SW2 versus energy. The dots in fig. 5 are values of C_M obtained using our analyzing program. The crosses are values obtained by subtracting spectra of the same series having different energies. This of course leaves a peak of quasi-monochromatic γ's. We plotted the peak channel position. A best fit of the points with a straight line gives an error on the extrapolated zero-energy position of (0.12 ± 0.3) and (0.06 ± 0.4) channels for SW1 and SW2 respectively.

3.3. Calibration and thresholds using GB spectra

Our method for determining the detection threshold requires the GB spectra of the counters to be analyzed. A typical spectrum, obtained during an experimental run at the energy of 1 GeV is shown in fig. 6, superimposed on the theoretical spectrum normalized at the plateau. A slight discrepancy, never exceeding 3% at the lowest end of the spectrum, between theoretical and experimental shape can be observed. It is important to note that, upon discovering this effect, we dismantled the whole electronics and rebuilt it more carefully: in particular a different type of linear gate was adopted. The change had no effect on the pulse height distribution. We are therefore reasonably confident that the discrepancy cannot be attributed to the electronics. The effect could of course be due mainly:

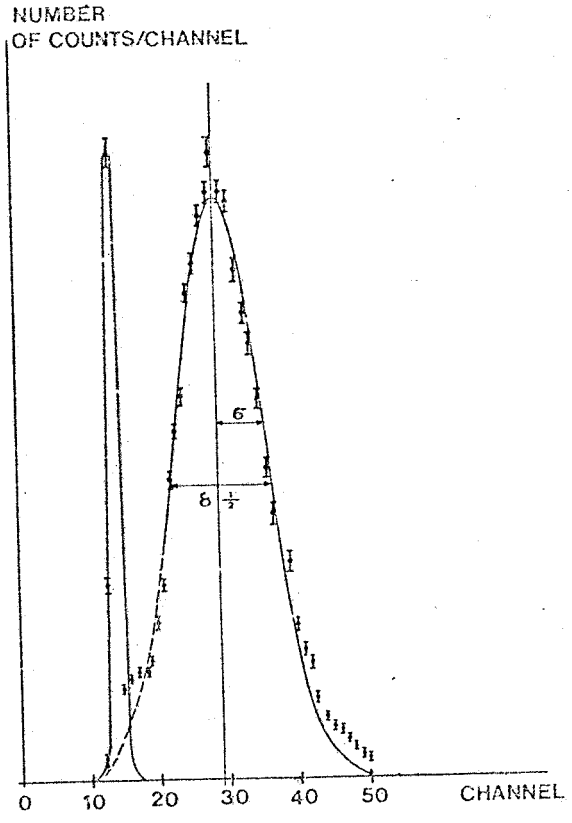

Fig. 8. Pulse-height distribution obtained with a monoenergetic electron beam. Beam energy 137 MeV.

a) to a non-linearity of our counters;
b) to a non-Gaussian distribution of the counter pulses for a monoenergetic beam;
c) to a physical effect causing a slight energy degrading of the spectrum [small effects of this kind are present (see section 6), but those we know of are not sufficient to explain the whole effect].

As described above, counter linearity was found to be within the experimental errors in the range 100–1200 MeV.

In order to check point (b) we have fitted test spectra obtained with a monoenergetic electron beam to Gaussian distributions. Figs. 8 and 9 show the distributions obtained at energies of 137 MeV and 250 MeV, respectively. At a level of 10% of the maximum height the asymmetry is less than 5%, and is not sufficient to explain the observed discrepancy.

The tentative conclusion we reach is that at least some background of low-energy γ's is produced inside the vacuum chamber. We could not, however, prove this point by direct measurement. Should the effect be due to a non-linearity of our system alone, it would be just barely compatible with our estimated maximum errors.

Reflections of this small discrepancy on our threshold values will be discussed in the paragraph on experimental errors.

3.4. Tagging of photons as a check on the energy calibration

A small ($1\times1\times1$ cm^3) plastic scintillator counter was installed inside bending magnet M10 (see fig. 1). The two quadrupoles and part of the magnet act as a momentum analyzer for electrons accompanying bremsstrahlung γ's. The γ and the accompanying electron (of known energy) can thus be detected in coincidence. If the accepted momentum byte is small enough, the associated γ's are quasi-monochromatic.

Our counter was placed at (6 ± 0.06) magnetic degrees inside the magnet, at a distance of (12 ± 1) cm from the equilibrium orbit. Taking into account the closed orbit position and angle, the peak of the γ-ray distribution was calculated to be at

$$\varepsilon = 0.85\pm0.01.$$

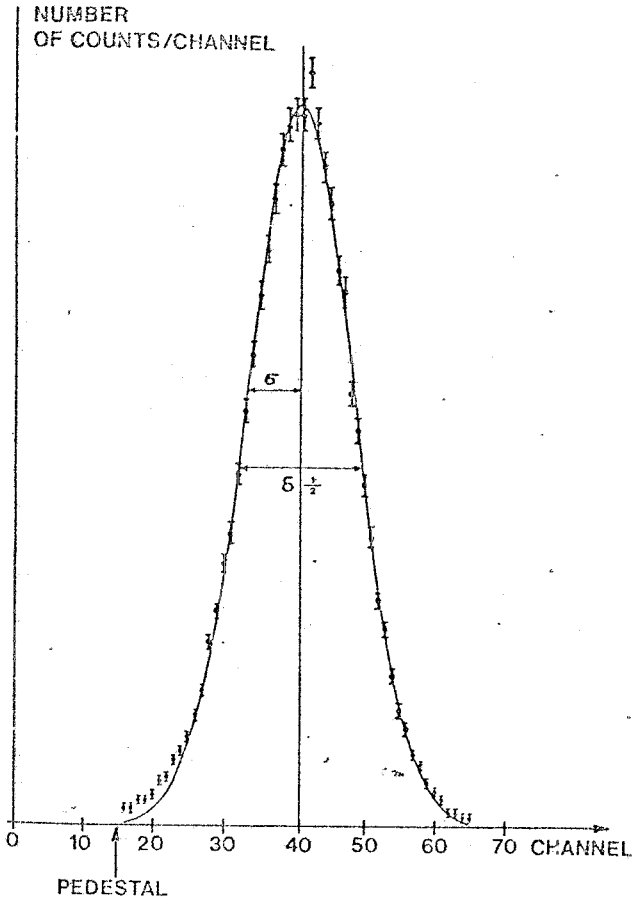

Fig. 9. Pulse-height distribution obtained with a monoenergetic electron beam. Beam energy 250 MeV.

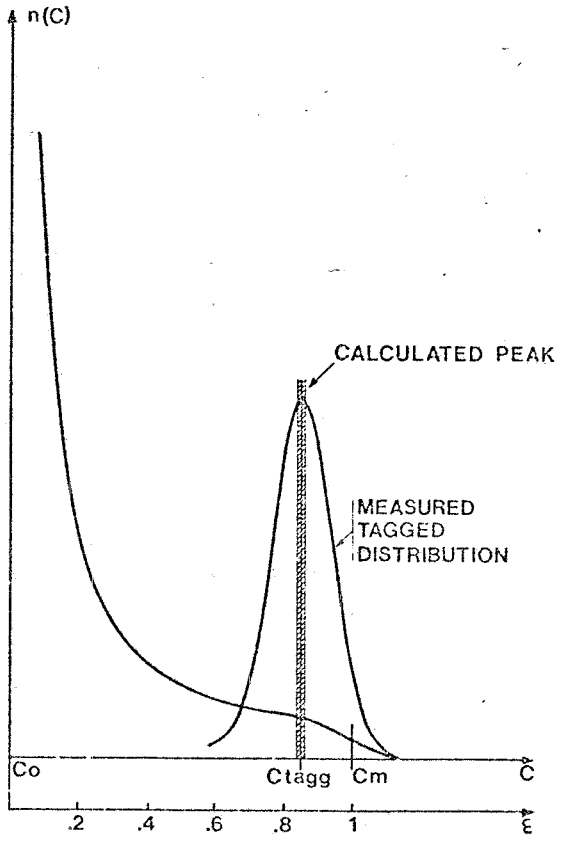

Fig. 10. Bremsstrahlung spectrum compared with tagged spectrum (amplified).

The error quoted is a mean square standard deviation. Fig. 10 shows one of the measured peaks. The test was performed at a machine energy of 1 GeV. The width of the peak corresponds to the 850 MeV resolution of the sandwich counter, since the resolution of the tagging system ($\Delta p/p \approx 3\%$ fwhm) is much better than that of the counter (24% fwhm). The calculated position of the peak agrees, well within the errors, with that estimated using method (a).

4. Background subtraction for single bremsstrahlung

As discussed in ref. 4 the main source of background to SB measurements is bremsstrahlung on the residual gas (GB). The signal-to-background ratio can easily be as low as 10%, so that subtraction requires special care. Background calculations are of course unreliable, since the average of pZ^2 (the product of the pressure and the mean square atomic number of the residual gas) over the path length seen by the apparatus is not well known and depends critically on machine conditions. Background measurements with spatially separated beams are also unreliable since, due to beam displacement, the desorption from the vacuum chamber walls changes and may cause large variations of pZ^2.

We therefore adopted the following method.

4.1. Missing-bunch method

Let us for convenience assume that telescopes T1 and T3 face the positron beam and that (in section 11) bunch j^+ collides with bunch j^- ($j = 1, 2, 3$). Let $i_k^{\pm}$ ($k = 1, 2, 3$) be the positron and electron bunch currents. The counting rate of T1, at interaction section 11, is given by

$$\dot{N}_k = G_k i_k^+ + S L_k (i_k^+ i_k^-), \qquad k = 1,2,3, \tag{2a}$$

and that of T3, at section 8, by

$$\dot{n}_k = g_k i_k^+, \qquad k = 1,2,3, \tag{2b}$$

where L is the luminosity produced by the collision of bunches k, while G_k, g_k and S are coefficients. G_k and g_k contain, besides the dominant GB term, background terms due to positrons lost on the vacuum chamber walls, while S is related to the cross section of SB. Obviously the total luminosity L is given by the sum of L_1, L_2, L_3.

Eqs. (2a) and (2b) are a system of six equations: in order to obtain the total luminosity L we must impose conditions on at least one bunch intensity, and make assumptions on the ratios of bunch currents in the two different straight sections.

Let us assume that bunch 3 of electrons is empty; then it follows immediately from eq. (2a) that

$$L = L_1 + L_2 = \frac{1}{S}\left[\dot{N}_1 + \dot{N}_2 - \dot{N}_3\left(\frac{G_1 i_1^+}{G_3 i_3^+} + \frac{G_2 i_2^+}{G_3 i_3^+}\right)\right]. \tag{3}$$

We now make the following assumptions

$$\frac{G_1}{G_3} = \frac{g_1}{g_3}, \qquad \frac{G_2}{G_3} = \frac{g_2}{g_3}. \tag{4}$$

From eqs. (2b), (3) and (4) we obtain

$$L = \frac{1}{S}\left[\dot{N}_1 + \dot{N}_2 - (\dot{N}_3/\dot{n}_3)(\dot{n}_1 + \dot{n}_2)\right]. \tag{5}$$

Under the further assumption that L be a function of the product of the colliding bunch currents only, namely

$$L = \text{const} \sum (i_k^+ i_k^-), \tag{6}$$

formula (5) can be generalized to the case where the third electron bunch current is not exactly zero. Under this assumption it is sufficient to correct the luminosity given by eq. (5), by a factor K defined as

$$K = \frac{\beta_2 + \alpha_3 + \alpha_2 \beta_3}{(\beta_2 - \beta_3) + \alpha_3 (1 - \beta_3)}, \tag{7}$$

where

$$\alpha_2 = i_2^+/i_1^+, \qquad \alpha_3 = i_3^+/i_1^+,$$
$$\beta_2 = i_2^-/i_1^-, \qquad \beta_3 = i_3^-/i_1^-. \tag{7}$$

Current ratios α_i and β_i can be accurately measured with vertically separated beams.

4.2. Checks

Since the method described in section 4.1 is based on several assumptions, accurate checks had to be performed.

Assumption (4) (independence of background ratios from the straight section where they are observed) was checked with one beam only, and with two separated beams under various machine operating conditions. The ratios $\dot{N}_k/\dot{N}_3$ and $\dot{n}_k/\dot{n}_3$ ($k = 1, 2$) were found to be the same to within the statistical errors (of the order of few tenths of a percent).

Assumption (6) can only be checked indirectly. The proof of the correctness of eq. (6) lies, in our opinion, in the fact that, while K ranges for our measurements between 1.0 and 1.2 (corresponding to 0–12% of the

intensity of the third bunch), no dependence of the ratio L_{DB}/L_{SB} on K has been observed: this is a good check because the correction applies to SB luminosity only (see fig. 15).

A further check on assumption (4) consists in fitting the experimental SB spectrum, obtained on a statistical basis from a spectrum containing both GB and SB γ's, to the theoretically expected curve. During several runs, the spectrum due to the e^+ bunch corresponding to the missing electron bunch, which is a pure GB spectrum, has been collected and subtracted from the total spectrum, after being normalized by the ratio of the currents, measured in the non-interaction section. An SB spectrum obtained in this way is shown in fig. 11 superimposed on its theoretical shape: the agreement is rather good. The fact that SB spectra agree with the calculated shape better than GB spectra seems to support our previous conclusion that at least part of the effect is due to a background originating inside the vacuum chamber, which would of course be subtracted from the SB spectrum.

5. Double bremsstrahlung measurement

The main characteristics of the double bremsstrahlung process

$$e^+ + e^- \rightarrow e^+ + e^- + \gamma + \gamma$$

have been summarized in section 1.

During all our runs we have recorded SB and DB events at the same time, so that a meaningful comparison can be made between the two measurements. The statistical error on DB is much greater than that on SB, because of the slow counting rate, due to the cross section being about 10^3 times lower than that of SB, and to signal-to-background conditions. The error on the average luminosity over all runs, however, becomes quite small, allowing us to check the correctness of the correction procedures, by comparing the two measurements (see sections 4, 6 and 7). It should be pointed out that the effect of the error on the threshold determination has the same sign for both SB and DB, so that the agreement between the two measurements is not a strong check of threshold determination.

6. Correction for conversions

The γ-rays we detect traverse a 3 mm thick stainless-steel window placed inside the fringing field of the bending magnets, and go through the anticoincidence counter in front of the sandwich. The charged particles generated by the conversions in the window are partially swept away by the fringing field of the magnets, thereby allowing a small fraction (δ_3) of degraded γ-rays to be detected by the sandwich.

The fraction of the primary γ-ray beam, which converts in the window plus the anticoincidence counter*, was measured to be

$$\delta_1 + \delta_2 = (12.7 \pm 0.2)\%;$$

* The measurement also takes into account possible back-scattering effects.

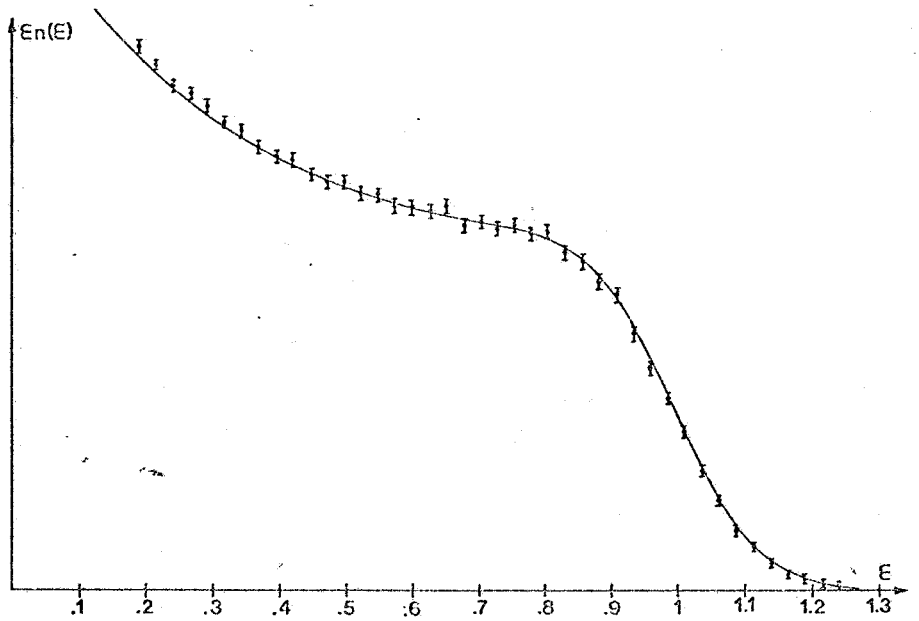

Fig. 11. Experimental single-bremsstrahlung spectrum compared with theoretical spectrum for SW1 Beam energy 1 GeV.

the contribution of the anticoincidence counter A1 being

$$\delta_2 = (2.5 \pm 0.2)\,\%,$$

and

$$\delta_3 = (1.0 \pm 0.2)\,\%.$$

The overall correction factor on the single bremsstrahlung rate is then:

$$f_{SB} = \frac{1}{1-(\delta_1+\delta_2-\delta_3)} = (1.133 \pm 0.005).$$

The corresponding factor for DB (A2 being slightly thicker than A1) was found to be

$$f_{DB} = (1.295 \pm 0.012).$$

The calculated value for δ_1 is 10.5%, which is in good agreement with the measured value.

7. Zero-luminosity check and correction

An overall test of the correctness of our background subtraction procedure is a measurement of SB and DB luminosity with two vertically separated beams. Beam separation was ≈ 10 mm, corresponding to ≈ 15 standard deviations. These "background" measurements have been performed at several energies and signal-to-

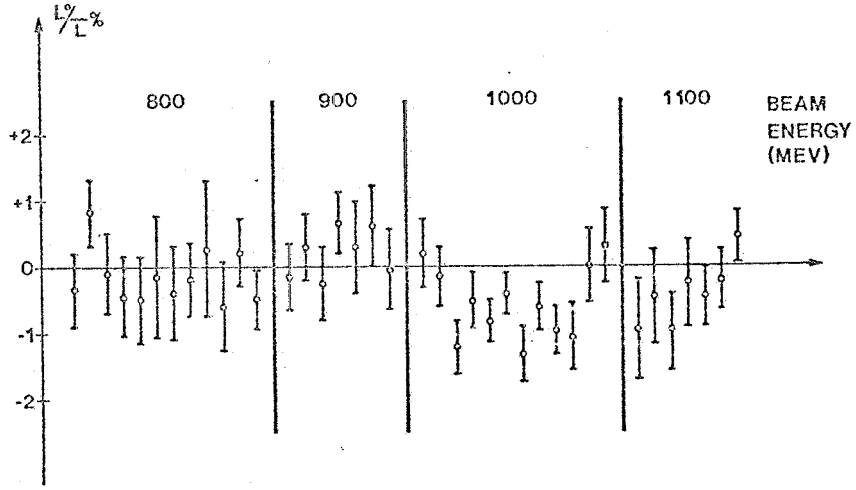

Fig. 12. Separated beams "background" luminosity; single bremsstrahlung.

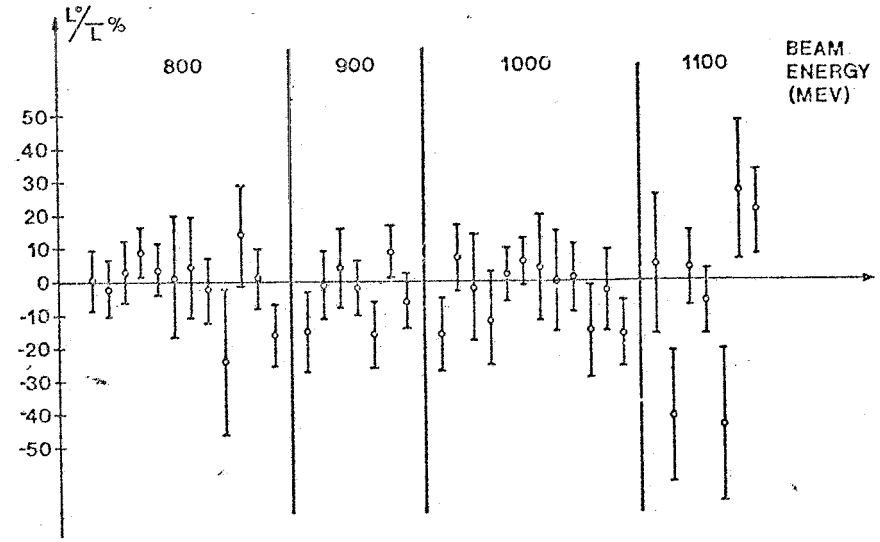

Fig. 13. Separated beams "background" luminosity; double bremsstrahlung.

background ratios, and are shown in figs. 12 and 13 for SB and DB, respectively. We have plotted the ratio of luminosity measured with vertically separated beams to that measured with crossing beams (L_0/L). The errors quoted are statistical.

In the case of DB most measurements show the background luminosity to be zero, independent of energy and signal-to-background ratio, within the statistical errors, which are of the order of 10–20% (see fig. 13). The average of the ratio L_0/L over all our runs is compatible with zero. Therefore no correction for this kind of background has been applied to DB luminosity.

In the case of SB all measurements of L_0/L lie within a range of $\pm 1.5\%$, the average over all runs being $(-0.35 \pm 0.11)\%$ (see fig. 12). There seems to be a slight variation of L_0/L with beam energy, and the fluctuations are of the order of 0.5%. This can in principle be expected, since residual gas pressure, currents and machine conditions are widely different at different energies and, as already mentioned, the precision of the measured ratio of bunch currents is of a few tenths of a percent. We have therefore corrected all SB luminosity measurements by 0.35% and increased the systematic error by $\pm 0.5\%$.

8. Errors

Luminosity is given by the general formula

$$L = \frac{\dot{N}_{(S+B)} - \dot{N}_B}{\sigma}, \qquad (8)$$

where $\dot{N}_{(S+B)}$ is the signal + background counting rate, $\dot{N}_B$ the background counting rate, and σ the effective cross section of the process being observed. This cross section is given by

$$\sigma_{SB} = \int_{\varepsilon_T}^{1} \int_{\Omega} \frac{d\sigma_{SB}(\varepsilon, 0, E_{max})}{d\varepsilon\, d\Omega}\, d\varepsilon\, d\Omega,$$

$$\sigma_{DB} = \int_{\varepsilon_{T1}}^{1} \int_{\varepsilon_{T2}}^{1} \int_{\Omega_1} \int_{\Omega_2} \frac{d\sigma_{DB}(\varepsilon_1, \varepsilon_2, 0_1, 0_2, E_{max})}{d\varepsilon_1\, d\varepsilon_2\, d\Omega_1\, d\Omega_2} \times$$

$$\times\, d\varepsilon_1\, d\varepsilon_2\, d\Omega_1\, d\Omega_2,$$

for SB and DB respectively, where ε_T and Ω are measured values, ε_T being the threshold energy and Ω the accepted solid angle.

Our results are affected by three kinds of errors:

(1) statistical errors due to fluctuations in counting rates;

(2) systematic errors due to uncertainties in the correction factors and in the evaluation of the integrated cross sections, which depends on measured quantities (ε_T, Ω);

(3) "random" errors which take into account variations of parameters relating counting rates to luminosity (beam position, threshold energy, etc.).

8.1. Single bremsstrahlung

As discussed in section 4, $\dot{N}_B$, the background counting rate, is given by

$$\dot{N}_B = \dot{N}_3 R,$$

$\dot{N}_3$ being the counting rate due to the e^+ bunch which interacts with the empty e^- bucket, and R being essentially proportional to an appropriate ratio of currents (see section 4). $\dot{N}_{S+B}$ and $\dot{N}_B$ are measured by the same telescope, so that all possible drifts are the same for both.

Aside from statistical errors, the only source of errors on the SB counting rate $(\dot{N}_{S+B} - \dot{N}_B)$ is the term R. The best check on the magnitude of any systematic error in the subtraction procedure is the measurement of luminosity with vertically separated beams. The results have been presented in section 7. We have assumed a systematic deviation of -0.35%, by which all measurements have been corrected: the error on this deviation is $\pm 0.5\%$, and it has been added to the systematic errors on L.

Our method for evaluating ε_T has been described in section 3. We have

$$\varepsilon_T = \frac{E_T}{E_{max}} = \frac{C_T - C_0}{C_M - C_0}.$$

C_T, C_M, C_0 are affected both by random and by systematic errors. The random error on C_T, C_M and C_0 is of the order of ± 0.1 channels at most. $(C_T - C_0)$ being of the order of 15, and $(C_M - C_0)$ of the order of 100, we find

$$(\Delta\varepsilon_T/\varepsilon_T)_{rnd} \approx \pm 1\%,$$

corresponding to an error on L of about $\pm 0.7\%$. As far as the systematic error on ε_T is concerned, we have taken the view of attributing the discrepancy between theoretical and experimental spectra to an actual energy degradation. If this were strictly true, our values for ε_T would be affected by the random error only. Since, however, the possibility of non-linearities or of a wrong estimate of the absolute position of C_0 cannot be entirely discarded, our values of ε_T could be affected by an error of approximately -4%. This last figure is a worst-case estimate. The corresponding systematic error on L is -2.7% at 800 MeV and -2.3% at 1100 MeV.

The collimators defining our apertures have been

positioned using the beam itself. Allowing for a ± 5 mm random beam displacement, the corresponding error on L is $+0.2\%$ at 800 MeV. Note that since our aperture is ± 6 mrad, L_{SB} is very insensitive to errors in the solid angle[4]).

As seen in section 6, our data have been corrected by the factor

$$f_{SB} = 1.133 \pm 0.005$$

on account of the conversions in the thick window. The corresponding systematic error of $\pm 0.5\%$ has been added to the other errors.

8.2. Double bremsstrahlung

The discussion just held on SB errors can be repeated for DB. Systematic errors on the two thresholds are approximately the same for the two telescopes T1 and T2, so that errors on L_{DB} are roughly about twice those on L_{SB}. Taking the shapes of the spectra into account in some more detail (SW2 shows a slightly better agreement between theoretical and experimental distributions than SW1), the systematic error on L_{DB} can be estimated to be -3.4% at 1100 MeV and -3.6% at 800 MeV. The random error on L_{DB} related to the evaluation of C_0, C_T and C_M is in this case $\pm 1\%$.

The solid angle, because of the different angular distribution of DB[4]), also gives rise to a larger random error. Under the same hypotheses already made for SB we find a maximum random error of $+0.5\%$. Allowing for a ± 6 cm error in the source–collimator distance, the corresponding error on L_{DB} is $\pm 0.2\%$.

The correction for the conversions in the thick window (see section 6) introduces a systematic error of $\pm 1.2\%$.

8.3. Overall error

The systematic and random errors described in sections 8.1 and 8.2 are summarized in table 1. Summing up all the systematic errors, and defining

$$\frac{\Delta L}{L} = \frac{L_{true} - L_{measured}}{L_{true}},$$

it is possible to define a "systematic error band" both for single and double bremsstrahlung. We obtain:

$$(-3.7 \leq (\Delta L/L)_{SB}^{syst} \leq 1.0)\,\%,$$

$$(-5.0 \leq (\Delta L/L)_{DB}^{syst} \leq 1.4)\,\%.$$

The same can be done for the random errors, which must be combined quadratically:

$$(\Delta L/L)_{SB}^{rnd} \approx \pm 0.8\%, \qquad (\Delta L/L)_{DB}^{rnd} \approx \pm 1.2\%.$$

The systematic and random error on the ratio $R = L_{DB}/L_{SB}$ is, however, smaller than the error on the individual measurements because, in most cases, the errors have the same effect on SB and DB measurements. The residual uncertainty on R is:

$$(-2.3 \leq (\Delta R/R)^{syst} \leq 1.4)\,\%,$$

$$(\Delta R/R)^{rnd} \approx \pm 1.0\%.$$

As far as radiative corrections are concerned, see section 9.

9. Results

We have measured SB and DB luminosity, in parallel with the small angle scattering (SAS) luminosity monitor[1]) during one week approximately (27/3/1972–1/4/1972) at the energies of 800, 900, 1000 and 1100 MeV. The SAS monitor is placed on the straight section where SB and DB are measured, so that a direct comparison between the two methods is possible.

A run typically consists of several points, in between two "separated beams" measurements. The latter were used both to collect GB spectra for threshold calibration purposes and to measure "zero luminosity" points

Table 1

Correction factors and errors in single and double bremsstrahlung measurements.

	SB			DB		
	Correction factor	Systematic error	Random error	Correction factor	Systematic error	Random error
Conversion in the thick window	1.133	$\pm 0.5\%$		1.295	$\pm 1.2\%$	
Zero luminosity	1.035	$\pm 0.5\%$				
Threshold		-2.7%	$\pm 0.7\%$		-3.6%	$\pm 1.0\%$
Solid angle			$+0.2\%$			$+0.5\%$
Source–collimator distance					$\pm 0.2\%$	

and the correction for the residual current in the third electron bunch.

In the course of one week thresholds varied (at constant phototube voltage) by 4–5 MeV at most. Our accuracy in threshold determination is, however, much better than that, since thresholds were measured both at the beginning and at the end of each run, and their average taken as the run threshold.

A typical run is shown in fig. 14. Each point, labeled by a number on the horizontal axis (from 1 to 13 in this case), corresponds to a 1000 s luminosity measurement. Black dots are the SB points, while crosses and triangles are the DB and SAS points respectively. The errors quoted are statistical.

It can be seen from fig. 14 that SB luminosity, being affected by a negligible statistical error, is the best monitor for relative measurements. As an example, after the measurement at point 8, the machine focusing conditions were changed slightly, in order to obtain a higher luminosity, and it can be seen from fig. 14 that only SB has been clearly sensitive to the variation. Statistical errors on DB are in this case roughly twice those on scattering: this because the DB signal-to-background ratio decreases rapidly with increasing energy;

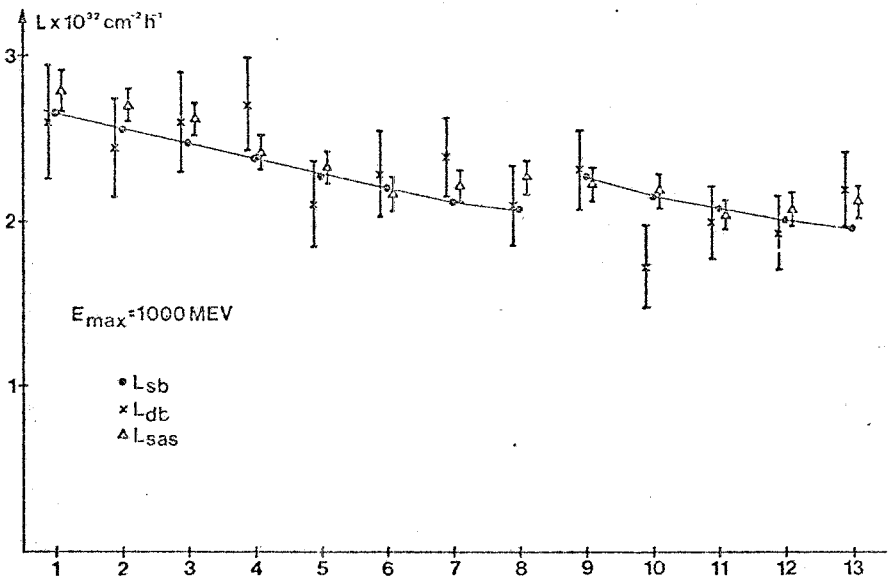

Fig. 14. Typical luminosity measurement run. Experimental points refer to 1000 s measurements.

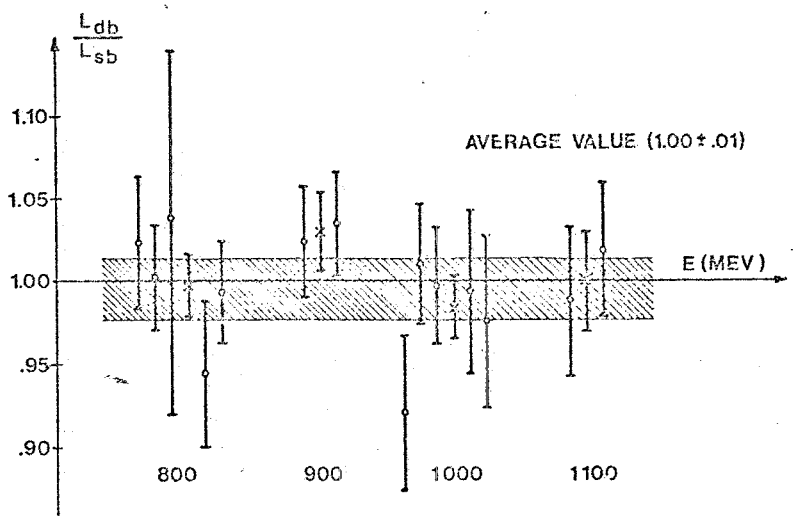

Fig. 15. Values of L_{DB}/L_{SB}. Crosses are the average values of the points at the same energy.

at 800 MeV statistical errors on DB and SAS are practically the same.

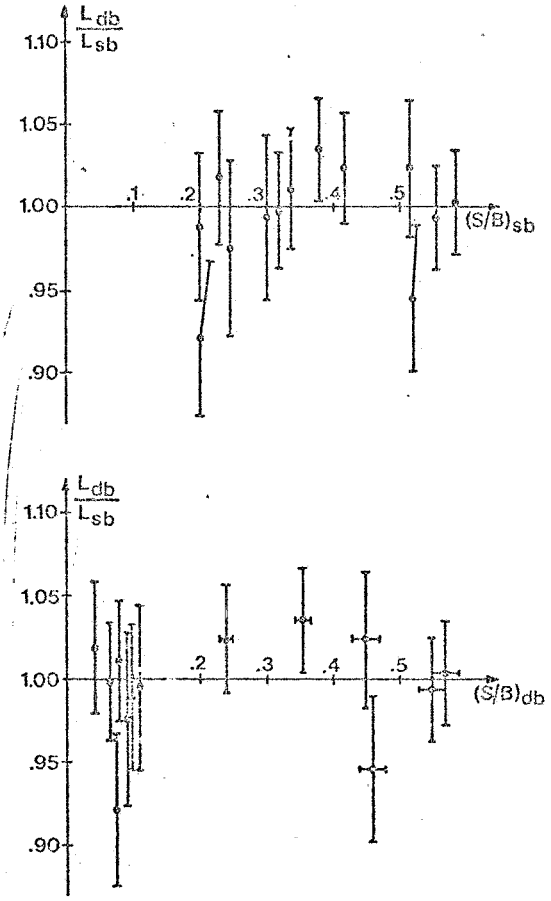

Fig. 16. L_{DB}/L_{SB} as a function of signal-to-background ratio; single and double bremsstrahlung.

Fig. 15 shows the value obtained for the ratio L_{DB}/L_{SB} over all our measurements, from 800 to 1100 MeV. Points are the average value of this ratio over individual runs (the crosses at the center of each group are the averages over all points at the same energy). The points appear to be statistically distributed around their average value of

$$L_{DB}/L_{SB} = 1.00 \pm 0.01,$$

which is well within our possible maximum estimated errors.

Fig. 16 shows the same points of fig. 15 as a function of the signal-to-background ratio of SB and DB respectively. No dependence of the result on these parameters is clearly apparent. In fig. 17 the same points are plotted versus K, the correction for the residual current in the third "missing" bunch (see section 4). Again no dependence of L_{DB}/L_{SB} on K is apparent: we conclude therefore that the background subtraction procedure described in section 4 is correct.

Fig. 18 shows the ratio of the luminosity measured by the SAS monitor to that measured by means of the SB reaction during the same runs; quoted errors are statistical. It has to be recalled that the SAS monitor is much more sensitive to machine conditions than both the SB and DB monitors. The scattering apparatus is in fact quite sensitive[7]) to longitudinal dimensions and to longitudinal and transverse position of the interaction region and to the closed orbit angle at the crossing point (this mostly because the machine is operating with head-on collisions). The main machine parameters involved are rf voltages, phases and frequency. These parameters can, to some extent, vary from one run to

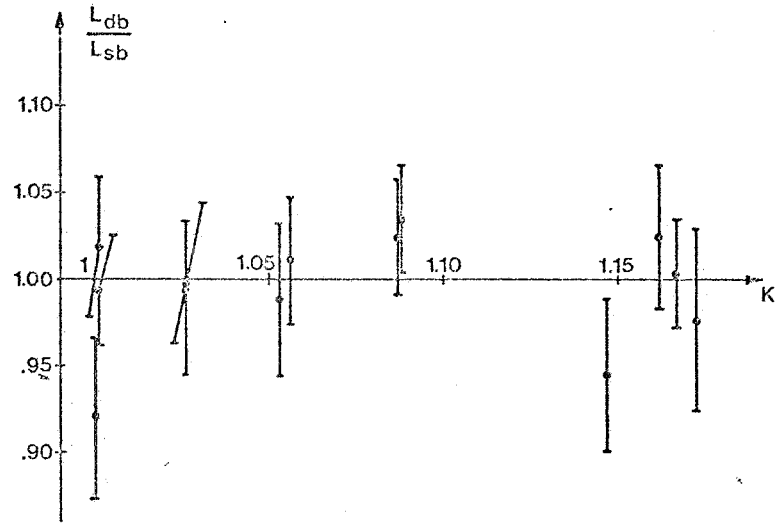

Fig. 17. L_{DB}/L_{SB} as a function of the correction K for the residual e^- bunch.

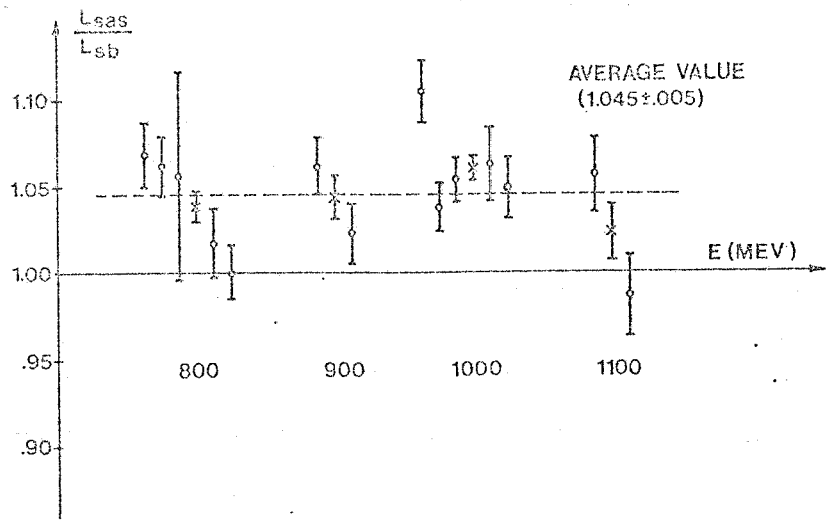

Fig. 18. Values of L_{SAS}/L_{SB}. Crosses are the average values of the points at the same energy.

the next, entailing a corresponding variation in the systematic errors on SAS luminosity. The small angle scattering cross section also depends on the absolute value of the beam energy. The distribution of the points around their average value shows that individual runs are affected by different systematic errors. The "average" value of the ratio L_{SAS}/L_{SB} (taking into account only statistical errors) is

$$L_{SAS}/L_{SB} = 1.045 \pm 0.005.$$

It has to be pointed out here, that, not having available a reliable estimate of the radiative corrections to be made on SB and on SAS, the data presented are not corrected for effects of this kind. The radiative corrections to DB have been calculated, in the soft photon approximation[10]), and turn out, in our case, to be +2.5% on luminosity. Radiative corrections to SB should be in the same direction, and a very rough estimate of radiative corrections on scattering seems to indicate that the corrections are of the same order of those to DB[11]) and in the opposite sense.

Considering the systematic error on SB, given in section 8, and the fact that systematic errors on SAS are of the same order as the above mentioned "average" deviation of the ratio L_{SAS}/L_{SB} from unity, it can be concluded that the two measurements are compatible with each other, within the expected systematic errors.

We thank the members of the group who have designed, built and operated the SAS monitoring system, and in particular F. Ceradini for collaborating during the runs and for providing us with the SAS data, and G. Nicoletti for constant technical assistance.

We are very grateful to all our colleagues of the Adone group for support and discussion, and in particular to M. Placidi and M. Vescovi for taking active part in collecting the data and for running the machine to our requirements.

References

1) G. Barbiellini, B. Borgia, M. Conversi and R. Santonico, Atti dell'Accademia Nazionale dei Lincei 44 (1968) 233; R. Santonico, Thesis (University of Rome); M. Preger, Thesis (University of Rome).
2) F. Amman, M. Bassetti, A. Cattoni, V. Chimenti, D. Fabiani, M. Matera, C. Pellegrini, M. Placidi, M. Preger, A. Renieri, S. Tazzari, F. Tazzioli and G. Vignola, 8th Intern. Conf. *High Energy Accelerators* (CERN, Geneva, 1971) p. 132.
3) F. Amman, *Dimensione dei fasci, vite medie, luminosita e caratteristiche della zona di interazione*, Frascati report LNF-66/6 (1966).
4) S. Tazzari, *Considerations on a luminosity monitor at Adone*, Frascati report LNF-67/23 (1967).
5) H. W. Koch and J. W. Motz, Rev. Mod. Phys. 31 (1959) 920.
6) G. Altarelli and F. Buccella, Nuovo Cimento 34 (1964) 1337.
7) P. Di Vecchia and M. Greco, Nuovo Cimento 50A (1967) 319.
8) E. Segré, *Experimental nuclear physics*, vol. 1, p. 260.
9) H. C. Dehne and M. Preger, *Numerical calculations on the small angle scattering luminosity monitor used at Adone*, Frascati report LNF-70/33 (1970).
10) V. N. Bayer and V. V. Geidt, Sov. J. Nucl. Phys. 13/2 p. 196.
11) M. Curatolo, Thesis (University of Rome).